



Cite this: Dalton Trans., 2025, 54, 13950

Received 8th August 2025,  
Accepted 2nd September 2025

DOI: 10.1039/d5dt01896j

rsc.li/dalton

## Introduction

Classic crown ethers like 18-crown-6 developed by Pedersen effectively bind metal cations within their polyether cavity (**I**, Scheme 1a – top).<sup>1–3</sup> In contrast, inverse crown ethers inverse this concept and trap anions within a cavity spanned by metal cations (**II**, Scheme 1a – bottom). Seminal reports by Mulvey and coworkers describe the serendipitous self-assembly of inverse crown ethers by reaction of  $\text{Na}^n\text{Bu}$ ,  $\text{Mg}^{(n)}\text{Bu}_2$  and  $\text{HN}^n$  ( $\text{N}^n = [\text{N}(\text{SiMe}_3)_2]^-$ ) and small quantities of oxygen impurities like  $\text{O}_2$  or  $\text{H}_2\text{O}$ .<sup>4,5</sup> Such complexes are generally formed in low yields and often mixtures of oxides and peroxides are obtained. These initial investigations have been extended to capturing more complex moieties within the metal crown, enabling the synthesis of unique multi-anionic products that are not accessible by standard deprotonation methods.<sup>6</sup>

Although the first inverse crown ethers with  $\text{O}^{2-}$  core anions have been extensively investigated, similar metal crown complexes with heavier chalcogenide anions ( $\text{S}^{2-}$ ,  $\text{Se}^{2-}$ ,  $\text{Te}^{2-}$ ) have so far not been reported. There is in general a lack of information on polar *s*-block metal complexes with heavy chalcogenides. The Cambridge Crystallographic Database contains only three crystal structures of *s*-block metal complexes with sulfide anions, *i.e.* complex **III-S** (Scheme 1b) and solvates thereof.<sup>7,8</sup> For polar selenide complexes there are only two examples, **III-Se** and the scorpionate complex **IV** (Scheme 1b).<sup>8,9</sup> *s*-Block metal complexes with encapsulated

$\text{Te}^{2-}$  anions are completely unknown. There are rare reports for the more polar molecular aluminium complexes with heavier chalcogenide anions (*e.g.* **V-Ch**, Scheme 1b).<sup>10–12</sup> This lack of knowledge stands in strong contrast with transition metal chalcogenide chemistry for which complexes<sup>13–22</sup> and materials<sup>23</sup> have been well studied.

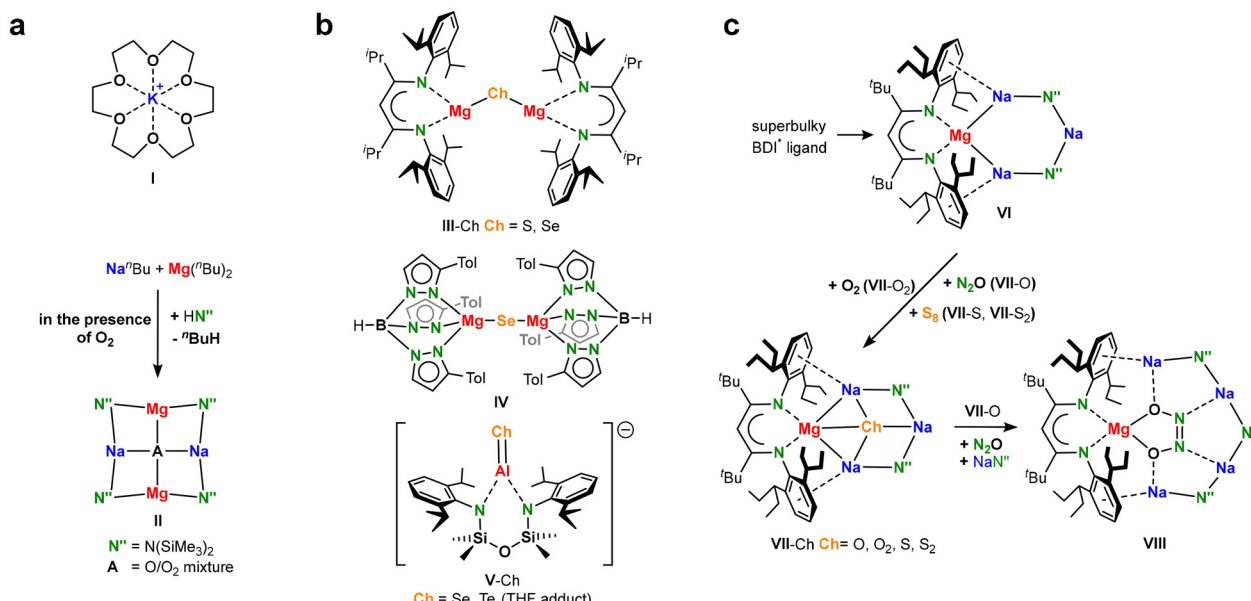
Herein, we present a unique “reduce-and-capture” concept to access ionic *s*-block metal complexes of the heavier chalcogenides  $\text{Ch}^{2-}$  anions. We recently introduced a redox-active metal crown complex (**VI**, Scheme 1c) that is able to reduce a substrate and encapsulate the resulting dianion.<sup>24</sup> This was exemplary shown for reaction with  $\text{N}_2\text{O}$  or epoxides, producing the  $\text{O}^{2-}$  anion, or for reaction with  $\text{O}_2$  to give an encapsulated peroxide dianion. Depending on stoichiometry, reactions with  $\text{S}_8$  resulted either in reduction to  $\text{S}^{2-}$  or formation of  $\text{S}_2^{2-}$ . Herein, we extend these investigations aiming to isolate complexes with a  $\text{Se}^{2-}$  anion, which are rare, or a  $\text{Te}^{2-}$  anion, which are hitherto unknown. As the ionic radii of the  $\text{Ch}^{2-}$  dianions gradually increase from  $\text{O}^{2-}$  (1.40 Å) over  $\text{S}^{2-}$  (1.84 Å) and  $\text{Se}^{2-}$  (1.98 Å) to  $\text{Te}^{2-}$  (2.21 Å) by almost 58%,<sup>25</sup> we were particularly interested whether capturing these larger anions requires ring extension. We also discuss trends in crystal structures, discuss solution dynamics and support our findings with DFT calculations.

## Results and discussion

Phosphine chalcogenides,  $\text{R}_3\text{P}=\text{Ch}$ , have been shown to be potent chalcogen transferring agents.<sup>8,10–12,26–32</sup> The key to this reactivity lies within the  $\text{P}=\text{Ch}$  bond which strictly speaking has more ylid ( $\text{P}^+\text{–Ch}^-$ ) than ylene character and weakens

Inorganic and Organometallic Chemistry, Friedrich-Alexander-Universität Erlangen-Nürnberg, Egerlandstraße 1, 91058 Erlangen, Germany.  
E-mail: sjoerd.harder@fau.de





**Scheme 1** (a) From Pedersen's crown ethers<sup>1–3</sup> to Mulvey's inverse crown complexes.<sup>4–6</sup> (b) Main group metal complexes with formal  $\text{Ch}^{+II}$  centres.<sup>8–11</sup> (c) The reduction of  $\text{O}_2$ ,  $\text{N}_2\text{O}$  or  $\text{S}_8$  with redox-active metal crown complex **VI**.<sup>24</sup>

going down group 16 ( $\text{P}=\text{O}$ : 130 kcal mol<sup>-1</sup>,  $\text{P}=\text{S}$ : 81 kcal mol<sup>-1</sup>,  $\text{P}=\text{Se}$ : 64 kcal mol<sup>-1</sup>,  $\text{P}=\text{Te}$ : 44 kcal mol<sup>-1</sup>).<sup>33</sup> Consequently, reduction of  $\text{R}_3\text{P}=\text{Ch}$  to the respective  $\text{R}_3\text{P}$  and  $\text{Ch}^{2-}$  fragments becomes easier along the row  $\text{Ch} = \text{O} < \text{S} < \text{Se} < \text{Te}$ .

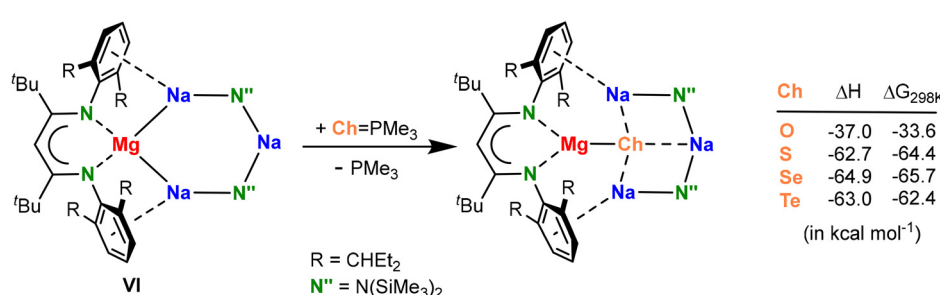
Use of  $\text{Ph}_3\text{P}=\text{Ch}$  reagents has been shown to be problematic in chalcogenide anion generation. The side-product  $\text{PPh}_3$  cannot be separated easily from the reaction mixture, culminating in a drastic decrease of isolated product yields.<sup>8</sup> Taking this into account, we chose to use  $\text{Me}_3\text{P}=\text{Ch}$  and  $\text{Et}_3\text{P}=\text{Ch}$  which have the advantage to produce volatile  $\text{PMe}_3$  and  $\text{PEt}_3$  which can be easily removed under vacuum. In all cases ( $\text{Ch} = \text{O, S, Se, Te}$ ), DFT calculations support the thermodynamic feasibility for the formation of  $(\text{BDI}^*)\text{MgNa}_3\text{N}^{+2}(\text{Ch})$  from **VI** and  $\text{Me}_3\text{P}=\text{Ch}$  (Scheme 2). The reaction with  $\text{Me}_3\text{P}=\text{O}$  is the least exothermic while the reductions of the heavier phosphine chalcogenides release nearly double this energy.

In a general procedure, a solution of the redox-active metal crown complex  $(\text{BDI}^*)\text{MgNa}_3\text{N}^{+2}$  (**VI**) in cyclohexane-*d*<sub>12</sub> was

reacted with one equivalent of  $\text{Me}_3\text{P}=\text{Ch}$  (or  $\text{Et}_3\text{P}=\text{Ch}$ ) at room temperature. Upon stirring, the dark red colour of the reaction mixtures usually turned to yellow, indicative of  $\text{Mg}^0$  to  $\text{Mg}^{+II}$  conversion. The volatiles, including the phosphine side-product, were removed under high vacuum and the selectivity of the reaction was checked by <sup>1</sup>H NMR.

### Formation and trapping of the oxide dianion (**VII-O**)

Whereas the reduction of  $\text{N}_2\text{O}$  with **VI** is facile and cleanly produced  $(\text{BDI}^*)\text{MgNa}_3\text{N}^{+2}(\text{O})$  (**VII-O**), the reaction of **VI** with one equivalent of  $\text{Me}_3\text{P}=\text{O}$  only led to 33% conversion. The other 66% of **VI** remained untouched. Addition of two more equivalents of  $\text{Me}_3\text{P}=\text{O}$  finally led to full conversion of **VI** into one major, yet unknown product, which according to <sup>1</sup>H NMR chemical shifts is not the expected  $(\text{BDI}^*)\text{MgNa}_3\text{N}^{+2}(\text{O})$  (**VII-O**). The observed proton spectrum is identical to that of the product formed in reaction of  $[(\text{BDI}^*)\text{Mg}]_2\text{Na}_2$  with two equivalents of  $\text{Me}_3\text{P}=\text{O}$  (SI Fig. S50). This indicates that upon addition of  $\text{Me}_3\text{P}=\text{O}$  the inverse crown template **VI** dis-



**Scheme 2** Calculated reaction enthalpies and free energies (kcal mol<sup>-1</sup>; B3PW91-GD3BJ/def2tzvp//B3PW91-GD3BJ/def2svp) for reaction of **VI** with  $\text{Me}_3\text{P}=\text{Ch}$  to metal crown complexes of the  $\text{Ch}^{2-}$  anions.

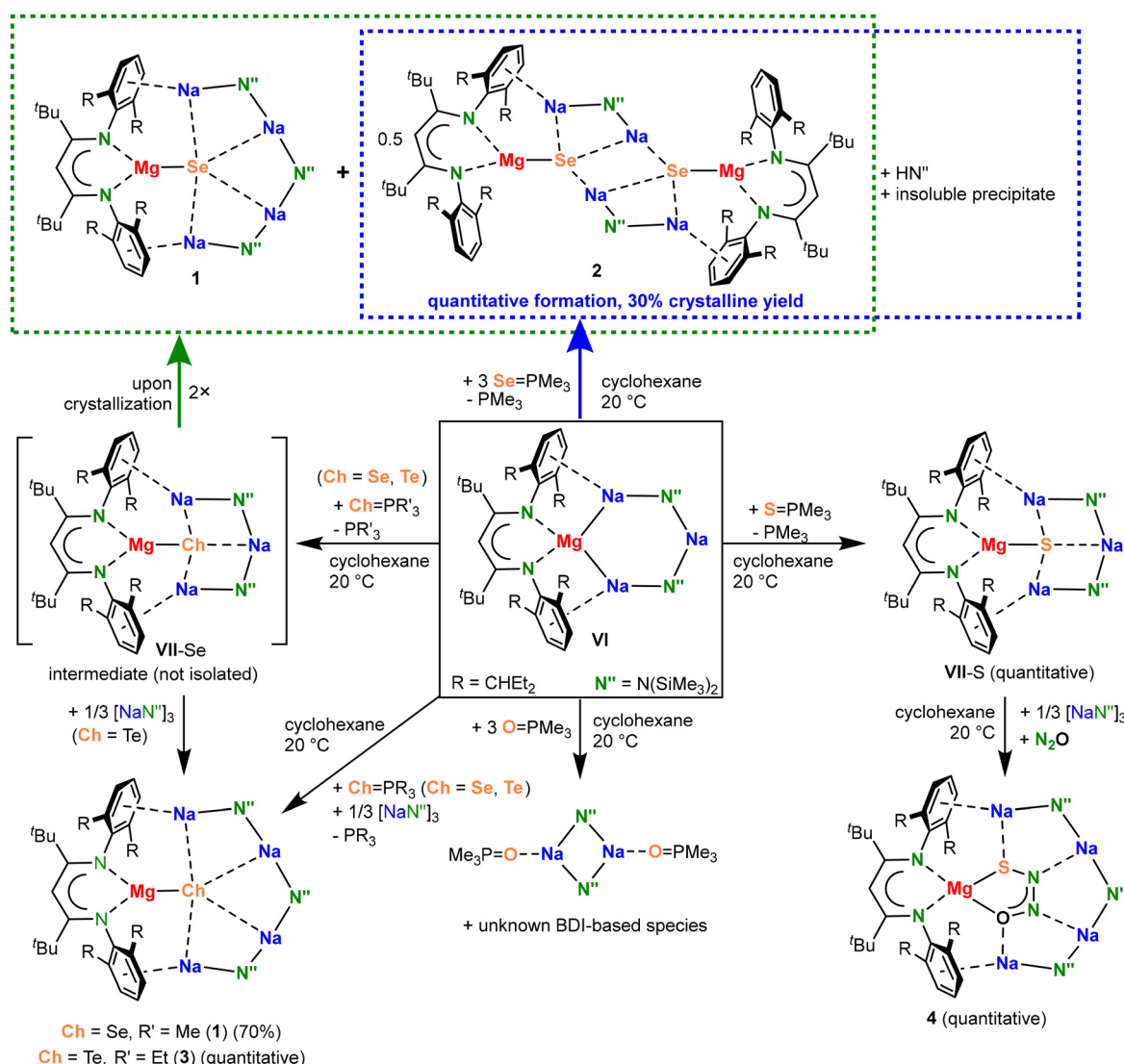
assembled and decomposed in  $[(\text{BDI}^*)\text{Mg}]_2\text{Na}_2$  and  $\text{NaN}''$  (Scheme 3). This is supported by NMR spectroscopy and X-ray diffraction analysis which are consistent with formation of  $[(\text{NaN}'')(\text{Me}_3\text{P}=\text{O})]_2$  (SI, Fig. S55). We earlier reported that **VI** disintegrates when dissolved in polar solvents as for example THF. Like THF,  $\text{Me}_3\text{P}=\text{O}$  can act like a polar solvent, resulting in disassembly of **VI** and isolation of  $[(\text{NaN}'')(\text{Me}_3\text{P}=\text{O})]_2$ .

### Formation and trapping of the sulfide dianion (**VII-S**)

Exchange of  $\text{Me}_3\text{P}=\text{O}$  for the much less polar phosphine sulfide reagent,  $\text{Me}_3\text{P}=\text{S}$ , led to clean oxidation of **VI** and exclusive formation of  $(\text{BDI}^*)\text{MgNa}_3\text{N}''_2(\text{S})$  (**VII-S**) and  $\text{PMe}_3$  (Scheme 3). Removing the solvent and phosphine under high vacuum gave a quantitative yield of essentially pure **VII-S** without the need of any further purification steps. Quantitative formation of the sulfide complex stands in contrast with the

modest yields reported for the reduction of  $\text{Mg}^1$  complexes with  $\text{Ph}_3\text{P}=\text{S}$ .<sup>8</sup> Clean reactivity to **VII-S** can be explained by the stabilizing influence of the metal crown. In addition,  $\text{Me}_3\text{P}=\text{S}$  is much less polar than  $\text{Me}_3\text{P}=\text{O}$  and not able to destroy the metal crown by coordination.

The oxidation of  $\text{Mg}^0$  in **VI** with  $\text{Me}_3\text{P}=\text{S}$  is the privileged route for the generation of the sulfide complex **VII-S**. In the previously reported procedure,<sup>24</sup> it was found critical to react **VI** with exactly 0.125 equivalents of  $\text{S}_8$  at low temperatures and at high dilution in order to prevent the formation of the persulfide complex  $(\text{BDI}^*)\text{MgNa}_3\text{N}''_2(\text{S}_2)$  (**VII-S<sub>2</sub>**). Especially on a smaller scale, it was found difficult to exactly add stoichiometric quantities of sulfur. The current synthetic route can be conveniently carried out in cyclohexane at room temperature using an excess of  $\text{Me}_3\text{P}=\text{S}$ . Any unreacted  $\text{Me}_3\text{P}=\text{S}$  remains as an insoluble solid which can be simply removed from the soluble product **VII-S** by filtration.



**Scheme 3** Reactivity of **VI** with phosphine chalcogenides  $\text{Ch}=\text{PMe}_3$  ( $\text{Ch}=\text{O, S, Se}$ ) and  $\text{Te}=\text{PEt}_3$ .



## Formation and trapping of the selenide and telluride dianions (1, 2, 3)

As  $R_3P=Se$  and  $R_3P=Te$  are both even less polar than  $R_3P=S$  and the  $P=Se$  and  $P=Te$  bonds are weaker than the  $P=S$  bond, controlled reduction of these reagents with **VI** should be straightforward.

The reduction of  $Me_3P=Se$  with **VI** led to the formation of various species among which complexes **1** and **2** are the main Mg selenide products (Scheme 3; raw product: Fig. S24 and S25). We presume that in a first step the expected product **VII**-Se is formed. However, in contrast to  $O^{2-}$  and  $S^{2-}$ , the  $Se^{2-}$  dianion is too large to comfortably fit in the  $(BDI^*)MgNa_3N''_2$  crown. Concentrating and cooling the mother liquor led to crystallization of a ring enlargement product in which an additional  $NaN''$  is built in the ring:  $(BDI^*)MgNa_4N''_3(Se)$  (**1**). Consequently, also a ring shrinkage product was found  $(BDI^*)MgNa_2N''(Se)$  which crystallised as a dimer (**2**). As **1** and **2** are both well soluble in alkanes, purification by crystallization and washing procedures only resulted in very low yields. However, as shown in the synthesis of  $(BDI^*)MgNa_4N''_3(ONNO)$  (**VIII**), ring expansion can be easily achieved by addition of 0.33 equivalents of trimeric  $(NaN'')_3$  to the reaction mixture.<sup>24</sup> Using the same approach, complex **1** could be isolated as a pure compound in 70% crystalline yield. We also observed that using a three-fold excess of  $Me_3P=Se$ , **VI** reacts selectively to **2**, the complex depleted of  $NaN''$ , which could be crystallized in 30% yield. This may be explained by the observation that  $(NaN'')_3$  itself also reacts with  $Me_3P=Se$  to give a highly insoluble white solid (likely  $Na_2Se_2$ ) and  $HN''$  in which the origin of the proton remains unexplained. Using excess  $Me_3P=Se$  thus removes  $NaN''$  from **VI**, resulting in more selective formation of **2** which is depleted by one  $NaN''$  unit. Thus, also complex **2** could be obtained pure and was after crystallization isolated in 30% yield. Complexes **1** and **2** both exhibit  $^{77}Se$  NMR signals with highly negative chemical shifts (**1**: -821.8 ppm, **2**: -828.3 ppm; referenced to  $SeMe_2$  as 0 ppm). These signals are considerably highfield-shifted when compared to Stasch's magnesium selenide complex **III**-Se (-764 ppm).<sup>8</sup> Complex **1** should show two different  $^1H$  NMR signals in a 2 : 1 ratio for the unequal  $N''$  ligands. The appearance of one signal indicates fast exchange between these

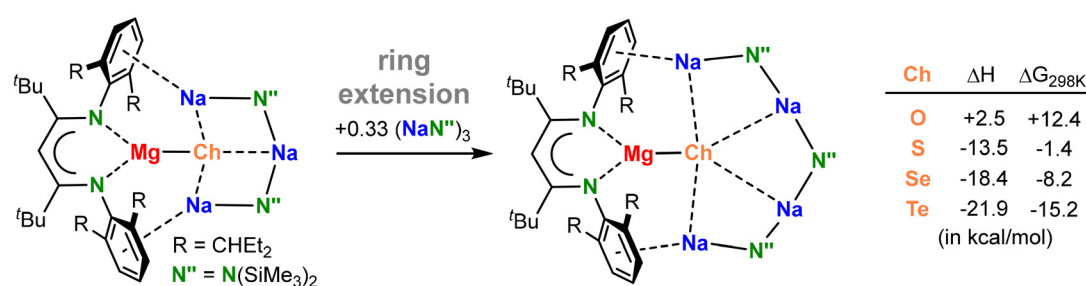
ligands. At -70 °C the signal broadens but decoalescence is not reached (Fig. S12).

In case of Te, we used  $Et_3P=Te$  as a reagent. The phosphine telluride  $Me_3P=Te$  is relatively unstable and easily decomposes to  $Me_3P$  and elemental Te. In contrast, the bulkier  $Et_3P=Te$  shows enhanced stability and  $PEt_3$ , which upon reduction is formed as a side-product, is still volatile enough for convenient removal under high vacuum. Reduction of  $Et_3P=Te$  with **VI** led to the isolation of the ring extension product ( $BDI^*)MgNa_4N''_3(Te)$  (**3**, Scheme 3). In this case, the ring shrinkage product could not be isolated or identified, probably due to poor stability. As discussed above, addition of 0.33 equivalent of trimeric  $(NaN'')_3$  at the start of the experiment, led to clean formation of the extended ring product and **3** could now be isolated in essentially quantitative yield. Similarly to the NMR shifts observed for the central  $Se^{2-}$  cores in **1** and **2**, the  $^{125}Te$  NMR spectrum of **3** features a noticeable high-field shifted resonance at -1902.3 ppm (referenced to  $TeMe_2$  as 0 ppm). Depending on the substituents,  $TeR_2$  compounds generally show  $^{125}Te$  resonances between 0 and 500 ppm. The very negative chemical shift measured for **3** is also *circa* 500 to 1000 ppm more upfield than aluminium based tellurides with both single and double bonded Al-Te moieties.<sup>12,34</sup> Complex **3** should show two different  $^1H$  NMR signals in a 2 : 1 ratio for the unequal  $N''$  ligands. The appearance of one signal indicates fast exchange between these ligands. At -70 °C the signal broadens but decoalescence is not reached (Fig. S37).

These investigations show that for the smaller chalcogenides,  $O^{2-}$  and  $S^{2-}$ , the optimal ring size is defined by a tetrametallic  $MgNa_3$ -crown. The larger chalcogenides,  $Se^{2-}$  and  $Te^{2-}$ , require the extended pentametallic  $MgNa_4$ -crown. DFT calculations, concerning such ring extension show that  $O^{2-}$  encapsulation indeed prefers the smaller ring (Scheme 4 and Fig. S56) whereas the free energy difference for  $S^{2-}$  encapsulation in a small or large ring is close to zero. Ring extension for the larger anions,  $Se^{2-}$  and  $Te^{2-}$ , becomes more exergonic with increasing anion size.

## Reactivity of metal crown chalcogenide complexes with $N_2O$

Inspired by the ring extension from a  $MgNa_3$ -ring in  $(BDI^*)MgNa_3N''_2(O)$  (**VII**-O) to the  $MgNa_4$ -ring in the hyponitrite complex  $(BDI^*)MgNa_4N''_3(ONNO)$  (**VIII**) (Scheme 1),<sup>24</sup> com-



**Scheme 4** Calculated reaction enthalpies and free energies (kcal mol<sup>-1</sup>; B3PW91-GD3BJ/def2tzvp//B3PW91-GD3BJ/def2svp) for ring extension by addition of 0.33 equivalent of  $(NaN'')_3$ .

plexes **VII-S**, **1** and **3** were exposed to an  $N_2O$  atmosphere. In all three cases, the  $^1H$  NMR spectra showed complete conversion of the reactants, but only for **VII-S** quantitative formation of the thiohyponitrite complex  $(BDI^*)MgNa_4N''_3(SNNO)$  (**4**) was observed. Reaction of **1** and **3** with  $N_2O$  led to mixtures containing a myriad of products which could not be further isolated or identified. Complex **4** is a rare thiohyponitrite complex and the first isolated complex with a *cis*-SNNO<sup>2-</sup> dianion trapped exclusively by main group metal cations.<sup>35,36</sup> Complex **4** should show three different  $^1H$  NMR signals in a 1:1:1 ratio for the unequal  $N''$  ligands. The appearance of one signal indicates fast exchange between these ligands. At  $-70^\circ C$  decoalescence is reached (Fig. S45).

### Crystal structures

Complex **1** crystallized  $C_2$ -symmetric with the two-fold symmetry axis through the ligand backbone-CH, Mg, Se and one of the amide N atoms (Fig. 1a). The analogous Te complex **3** is

approximately  $C_2$ -symmetric but does not possess crystallographic symmetry (Fig. 1b). The common feature of both compounds is the eight-membered Mg–Na–N–Na–N–Na–N–Na ring encapsulating the  $Ch^{2-}$  dianion. In contrast to **VI** in which the ring is held together by Mg–Na and Na–N bonds, the rings in **1** and **3** are formed by Ar–Na and Na–N bonding. While the Mg–Na bonds in **VI** are in the range of 3.261(2)–3.407(2) Å, the non-bonding Mg–Na1 distances in **1** measure 3.6568(6) Å. Those in **3** are slightly longer: 3.896(1)–3.951(1) Å. The latter lie within the range of the expanded metal crown complex **VIII** (Mg–Na 3.927(1)–3.965(1) Å). The Ar(centroid)–Na contacts in **1** and **3** vary from 2.625(1) to 2.705(1) Å and are of comparable length as similar interactions in **VI** (2.626(2)–2.735(2) Å) or **VIII** (2.600(1)–2.639(1) Å).<sup>24</sup>

The Mg–Ch bonds of 2.4141(6) Å in **1** and 2.6068(6) Å in **3** are much shorter than the comparable Na–Ch distances varying from 2.8792(5) to 3.0084(6) Å in **1** or 3.0629(8) to 3.2259(8) Å in **3**. The Mg–Ch bonds in **1** and **3** are also shorter

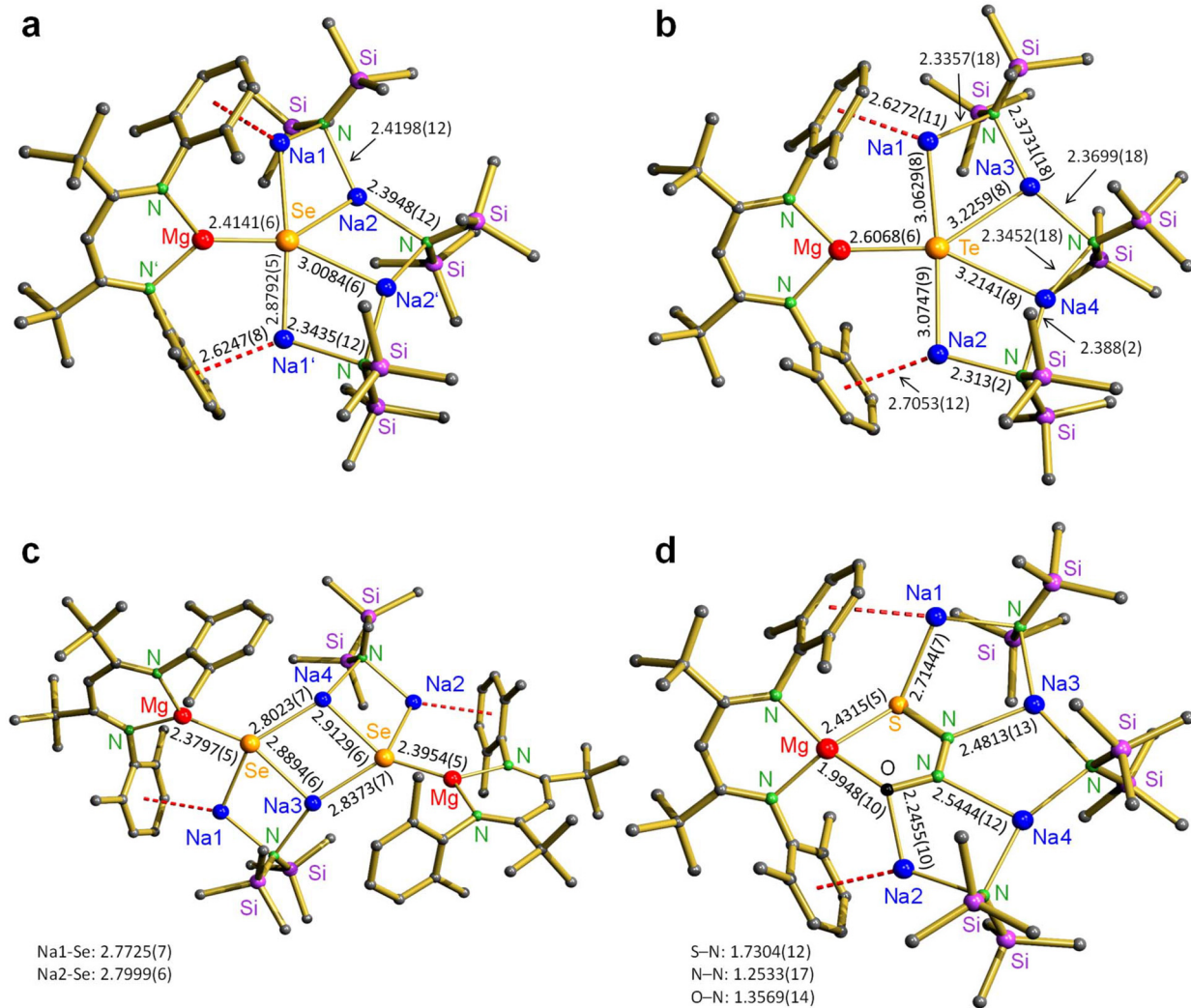


**Fig. 1** Crystal structures; Et groups of the  $Et_2CH$ -substituents and H atoms are not shown for clarity. Bond distances shown in Å. (a)  $(BDI^*)MgNa_4N''_3(Se)$  (**1**). (b)  $(BDI^*)MgNa_4N''_3(Te)$  (**3**). (c)  $[(BDI^*)MgNa_2N''(Se)]_2$  (**2**). (d)  $(BDI^*)MgNa_4N''_3(SNNO)$  (**4**).

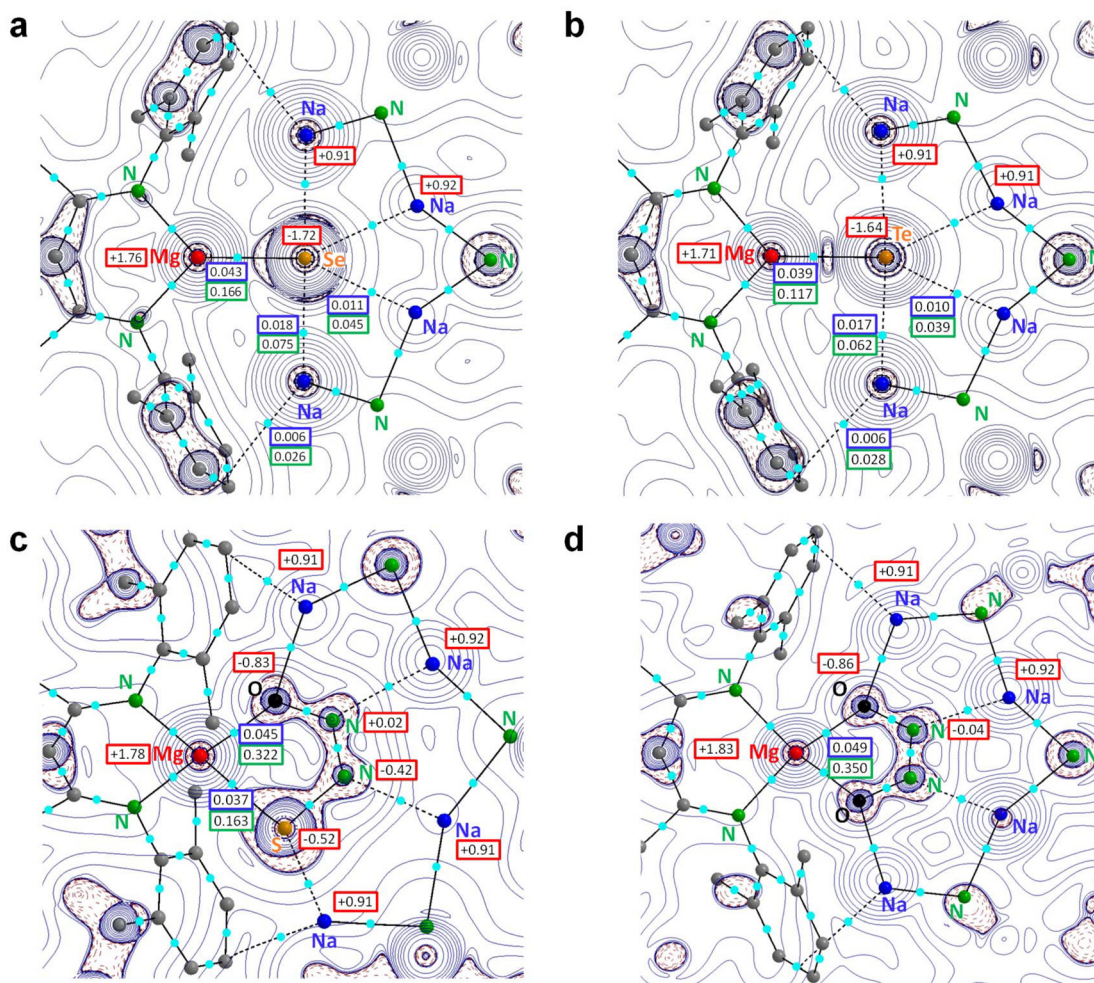


**Fig. 2** NPA and Atoms-in-Molecules analyses. The Laplacian distributions show bcp's (light-blue) with  $\rho(r)$  ( $e B^{-3}$  in blue boxes), the Laplacian  $\nabla^2\rho(r)$  ( $e B^{-5}$  in green boxes) and NPA charges (red boxes). (a)  $(BDI^*)MgNa_4N''_3(Se)$  (1). (b)  $(BDI^*)MgNa_4N''_3(Te)$  (3). (c)  $(BDI^*)MgNa_4N''_3(SNNO)$  (4). (d)  $(BDI^*)MgNa_4N''_3(ONNO)$  (VIII).

than the sum of the covalence radii for Mg and Ch (Mg + Se: 2.61 Å, Mg + Te: 2.79 Å).<sup>37</sup> Mg–Se distances of similar length are observed in Parkin's magnesium selenide complex **IV** (2.404(3) and 2.408(3) Å)<sup>9</sup> and Stasch's **III**–Se (2.3497(18)–2.4739(18) Å).<sup>8</sup> The hitherto only compound with a Mg–Te bond that is crystallographically characterized,  $Mg[TeSi(SiMe_3)_3]_2(THF)_2$ , features considerably longer contacts (2.714(1)–2.720(2) Å) than in **3**.<sup>38,39</sup> This is likely due to the mono-anionic nature of  $(Me_3Si)_3SiTe^-$  compared to dianionic  $Te^{2-}$ .

Complex **2** can be considered a dimer of  $(BDI^*)MgNa_2N''(Se)$  units in which  $Se^{2-}$  is bound to Mg and chelated by a  $Na-N''-Na$  arm. The dimer has no crystallographic symmetry but is close to being  $C_2$ -symmetric. The average Mg–Se (2.3876 Å) and Na–Se (2.8357 Å) distance in **2** are slightly shorter than those in **1** (average values: Mg–Se 2.4141 Å, Na–Se 2.9438 Å). This is due to the fact that  $Se^{2-}$  is five-coordinate in **1** but only four-coordinate in **2**.

The thiohyponitrite complex **4** (Fig. 1d) crystallizes similarly to the hyponitrite complex **VIII**.<sup>24</sup> It encapsulates a *cis*-SNNO<sup>2-</sup>

anion within an eight-membered Mg–Na1–N–Na3–N–Na4–N–Na2 ring and is bound by Mg–S, Mg–O, S–Na, O–Na and N–Na interactions. The O–N–N–S bond distances in **4** are (Å): 1.357(1)–1.253(2)–1.730(1). The O–N and N–N distances in **4** are very much comparable to those in the hyponitrite anion in complex **VIII** (O–N: 1.363(2), N–N: 1.261(2) Å), implying that replacement of O for S hardly influences O–N and N–N distances. In contrary, comparing the O–N–N–S bond distances in **4**, 1.357(1)–1.253(2)–1.730(1), with those in a  $\beta$ -diketiminate Zn thiohyponitrite complex, 1.229(6)–1.306(7)–1.793(5),<sup>35</sup> shows significant differences that are likely related to differences between ionic bonding in **4** versus the more covalently bonding character in the Zn complex.

### Computational studies

DFT calculations were conducted at the B3PW91-D3BJ/def2tzvp//B3PW91-D3BJ/def2svp level of theory which includes corrections for dispersion. The geometries for **1** and **3** have been optimized in  $C_2$ -symmetry. They are in agreement with

those obtained by X-ray diffraction and only minor discrepancies are noted. The calculated Ch–Na bond lengths (**1**: Na1 2.780 Å, Na2 2.986 Å; **3**: Na1/2 2.939 Å, Na3/4 3.132 Å) are slightly shorter than the experimentally found values (**1**: Na1 2.879 Å, Na2 3.008 Å; **3**: Na1/2 3.063–3.075 Å, Na3/4 3.214–3.226 Å).

Atoms-In-Molecules (AIM) analysis confirms bonding between Mg–Ch and Ch–Na through the identification of bond paths and bond-critical points (bcp's) along the Mg–Ch and Ch–Na axes (Fig. 2a and b). The electron density  $\rho(\mathbf{r})$  in the Mg–Ch bcp's is 2–4 times larger than in the Ch–Na bcp's underpinning the observations of X-ray diffraction, that Mg–Ch is the prominent bond. However, the associated electron density  $\rho(\mathbf{r})$  and Laplacian  $\nabla^2\rho(\mathbf{r})$  in the bcp's are in all cases low, indicating a mainly ionic interaction. The Laplacian of the electron distribution shows a concentration of electron density at the  $\text{Ch}^{2-}$  centres which is mainly polarized towards  $\text{Mg}^{2+}$  and only weakly directed to the nearest  $\text{Na}^+$  ions. The high electron density at the  $\text{Ch}^{2-}$  centres is further supported by Natural Population Analysis (NPA), which calculates a very low charge of  $-1.71$  at Se and  $-1.64$  at Te, and high positive charges at Mg (average  $+1.74$ ) and Na (average  $+0.91$ ), in line with ionic bonding between  $\text{Ch}^{2-}$ ,  $\text{Mg}^{2+}$  and  $\text{Na}^+$ .

Fig. 2c shows the Laplacian and charge distribution for the thiohyponitrite complex **4**. The  $\text{SNNO}^{2-}$  dianion is ionically bound in the metal crown with a total NPA charge of  $-1.75$ . The electron density on the Mg–S bond path is significantly smaller than that on the Mg–O bond path indicating that the Mg–O contact is the main bonding interaction.

Looking at the charge distribution within the thiohyponitrite anion (Fig. 2c) compared to that in the hyponitrite anion in **VIII** (Fig. 2d), it becomes clear that the latter has a major resonance form represented by  $\text{^O-N=N-O^-}$  whereas in thiohyponitrite there is charge delocalization:  $\text{^S-N=N-O^-} \leftrightarrow \text{^S-N^-N=O}$ . Both N atoms in  $\text{ONNO}^{2-}$  are nearly neutral whereas the N atom next to S in  $\text{SNNO}^{2-}$  carries a considerable negative charge.

## Conclusion

The redox-active inverse crown complex **VI** is not stable in the presence of  $\text{Me}_3\text{P=O}$ . This is likely due to the high polarity of this phosphine oxide reagent which leads to loss of  $(\text{NaN}^{\prime\prime})_2$  from **VI**, resulting in  $[(\text{NaN}^{\prime\prime})(\text{Me}_3\text{P=O})]_2$ , which could be identified, and  $[(\text{BDI}^*)\text{Mg}]_2\text{Na}_2$  which unselectively reduced  $\text{Me}_3\text{P=O}$  to a yet unidentified product. The much less polar heavier phosphine chalcogenides,  $\text{R}_3\text{P=Ch}$  (Ch = S, Se, Te), serve as excellent chalcogen transferring agents. Reduction of  $\text{R}_3\text{P=Ch}$  with the redox-active inverse crown **VI** led to inverse crown complexes with encapsulated  $\text{Ch}^{2-}$  dianions (**VII-S**, **1** and **3**). Choosing phosphine chalcogenides  $\text{R}_3\text{P=Ch}$  with  $\text{R} = \text{Me}$  or  $\text{Et}$  greatly simplified separation. Compared to solid  $\text{PPPh}_3$ , the volatile phosphines  $\text{PMe}_3$  and  $\text{PET}_3$  enabled high to quantitative product yields. Complex **VII-S** was previously prepared by reduction of  $\text{S}_8$  with **VI**. However, a slight excess of

elemental sulfur led to contamination of the sulfide product **VII-S** with the disulfide **VII-S<sub>2</sub>**. Since excess of  $\text{R}_3\text{P=S}$  does not disturb the clean formation of **VII-S**, this is the preferred method of preparation. The heavier chalcogenides  $\text{Se}^{2-}$  and  $\text{Te}^{2-}$  are too large to be sufficiently stabilized by the tetrametallic  $\text{MgNa}_3$ -crown and required the formation of an extended pentametallic  $\text{MgNa}_4$ -crown. This was achieved by simple addition of 0.33 equivalents of  $(\text{NaN}^{\prime\prime})_3$  to the reaction mixtures. Reaction of  $(\text{BDI}^*)\text{MgNa}_3\text{N}^{\prime\prime}_2(\text{S})$  (**VII-S**) with  $\text{N}_2\text{O}$  in the presence of 0.33 equivalents  $(\text{NaN}^{\prime\prime})_3$  quantitatively yielded an inverse crown complex with the rare thiohyponitrite dianion *cis*- $\text{SNNO}^{2-}$ . The high electron density is delocalized over the four heteroatoms and, apart from the  $\text{^S-N=N-O^-}$  resonance structure, features a significant  $\text{^S-N^-N=O}$  contribution. Current work focuses on expanding the scope of the reduce-and-capture properties of **VI** to other groups of the periodic table and various small molecules.

## Conflicts of interest

The authors declare no competing financial interest.

## Data availability

Supplementary information: synthetic procedures, selected NMR spectra, details for crystal structure determination, details for computational work. See DOI: <https://doi.org/10.1039/d5dt01896j>.

CCDC 2429354, 2429355, 2429356, 2387081 and 2449050 contain the supplementary crystallographic data for this paper.<sup>40a–e</sup>

## Acknowledgements

We acknowledge A. Roth for CHN analyses, M. A. Schmidt for support with the computational part and Dr. C. Färber and J. Schmidt for assistance with NMR analyses. We thank the Deutsche Forschungsgemeinschaft for funding (DFG: HA 3218/12-1).

## References

- 1 C. J. Pedersen, *J. Am. Chem. Soc.*, 1967, **89**, 7017–7036.
- 2 C. J. Pedersen, *Science*, 1988, **241**, 536–540.
- 3 C. J. Pedersen, *Angew. Chem., Int. Ed. Engl.*, 1988, **27**, 1021–1027.
- 4 A. R. Kennedy, R. E. Mulvey and R. B. Rowlings, *Angew. Chem., Int. Ed.*, 1998, **37**, 3180–3183.
- 5 R. E. Mulvey, *Chem. Commun.*, 2001, 1049–1056.
- 6 R. E. Mulvey, *Organometallics*, 2006, **25**, 1060–1075.
- 7 B. Li, C. Wölper and S. Schulz, CCDC 2290051. DOI: [10.5517/ccdc.csd.cc2gvyzny](https://doi.org/10.5517/ccdc.csd.cc2gvyzny).



8 S. Burnett, R. Ferns, D. B. Cordes, A. M. Z. Slawin, T. van Mourik and A. Stasch, *Inorg. Chem.*, 2023, **62**, 16443–16450.

9 P. Ghosh and G. Parkin, *Chem. Commun.*, 1996, 1239.

10 M. J. Evans, M. D. Anker, C. L. McMullin, N. A. Rajabi and M. P. Coles, *Chem. Commun.*, 2021, **57**, 2673–2676.

11 M. D. Anker and M. P. Coles, *Angew. Chem., Int. Ed.*, 2019, **58**, 13452–13455.

12 X. Zhang and L. L. Liu, *J. Am. Chem. Soc.*, 2023, **145**, 15729–15734.

13 W. A. Howard and G. Parkin, *J. Am. Chem. Soc.*, 1994, **116**, 606–615.

14 D. Rabinovich and G. Parkin, *Inorg. Chem.*, 1995, **34**, 6341–6361.

15 J. L. Kisko, T. Hascall and G. Parkin, *J. Am. Chem. Soc.*, 1997, **119**, 7609–7610.

16 C. Schneider, S. Ivlev and C. G. Werncke, *Eur. J. Inorg. Chem.*, 2023, **26**, e202200706.

17 W. Ren, G. Zi, D.-C. Fang and M. D. Walter, *J. Am. Chem. Soc.*, 2011, **133**, 13183–13196.

18 W. A. Howard, T. M. Trnka, M. Waters and G. Parkin, *J. Organomet. Chem.*, 1997, **528**, 95–121.

19 W. A. Howard and G. Parkin, *J. Organomet. Chem.*, 1994, **472**, c1–c4.

20 J. H. Shin and G. Parkin, *Organometallics*, 1994, **13**, 2147–2149.

21 J. H. Shin and G. Parkin, *Organometallics*, 1995, **14**, 1104–1106.

22 V. J. Murphy and G. Parkin, *J. Am. Chem. Soc.*, 1995, **117**, 3522–3528.

23 G. Giuffredi, T. Asset, Y. Liu, P. Atanassov and F. Di Fonzo, *ACS Mater. Au*, 2021, **1**, 6–36.

24 J. Maurer, L. Klerner, J. Mai, H. Stecher, S. Thum, M. Morasch, J. Langer and S. Harder, *Nat. Chem.*, 2025, **17**, 703–709.

25 R. D. Shannon, *Acta Crystallogr., Sect. A*, 1976, **32**, 751–767.

26 T. Chu, S. F. Vyboishchikov, B. Gabidullin and G. I. Nikonov, *Angew. Chem., Int. Ed.*, 2016, **55**, 13306–13311.

27 B. J. Reeves and B. M. Boardman, *Polyhedron*, 2014, **73**, 118–123.

28 S. M. Stuczynski, Y.-U. Kwon and M. L. Steigerwald, *J. Organomet. Chem.*, 1993, **449**, 167–172.

29 W. Imhof and G. Huttner, *J. Organomet. Chem.*, 1993, **448**, 247–253.

30 G. Hogarth, N. J. Taylor, A. J. Carty and A. Meyer, *J. Chem. Soc., Chem. Commun.*, 1988, 834–836.

31 D. Belletti, D. Cauzzi, C. Graiff, A. Minarelli, R. Pattacini, G. Predieri and A. Tiripicchio, *J. Chem. Soc., Dalton Trans.*, 2002, 3160–3163.

32 T. Chu, S. F. Vyboishchikov, B. M. Gabidullin and G. I. Nikonov, *Inorg. Chem.*, 2017, **56**, 5993–5997.

33 N. Sandblom, T. Ziegler and T. Chivers, *Can. J. Chem.*, 1996, **74**, 2363–2371.

34 H. Xu, A. Kostenko, C. Weetman, S. Fujimori and S. Inoue, *Angew. Chem., Int. Ed.*, 2023, **62**, e202216021.

35 N. J. Hartmann, G. Wu and T. W. Hayton, *Angew. Chem., Int. Ed.*, 2015, **54**, 14956–14959.

36 M. Á. Baeza Cinco, G. Wu, N. Kaltsosyannis and T. W. Hayton, *Angew. Chem., Int. Ed.*, 2020, **59**, 8947–8951.

37 B. Cordero, V. Gómez, A. E. Platero-Prats, M. Revés, J. Echeverría, E. Cremades, F. Barragán and S. Alvarez, *Dalton Trans.*, 2008, 2832.

38 D. E. Gindelberger and J. Arnold, *J. Am. Chem. Soc.*, 1992, **114**, 6242–6243.

39 D. E. Gindelberger and J. Arnold, *Inorg. Chem.*, 1994, **33**, 6293–6299.

40 (a) J. Maurer, L. Klerner, J. Langer, S. Harder, CCDC 2429354: Experimental Crystal Structure Determination, 2025, DOI: [10.5517/ccdc.csd.cc2mjy8d](https://doi.org/10.5517/ccdc.csd.cc2mjy8d); (b) J. Maurer, L. Klerner, J. Langer, S. Harder, CCDC 2429355: Experimental Crystal Structure Determination, 2025, DOI: [10.5517/ccdc.csd.cc2mjy9f](https://doi.org/10.5517/ccdc.csd.cc2mjy9f); (c) J. Maurer, L. Klerner, J. Langer, S. Harder, CCDC 2429356: Experimental Crystal Structure Determination, 2025, DOI: [10.5517/ccdc.csd.cc2mjybg](https://doi.org/10.5517/ccdc.csd.cc2mjybg); (d) J. Maurer, L. Klerner, J. Langer, S. Harder, CCDC 2387081: Experimental Crystal Structure Determination, 2025, DOI: [10.5517/ccdc.csd.cc2l3ym9](https://doi.org/10.5517/ccdc.csd.cc2l3ym9); (e) J. Maurer, L. Klerner, J. Langer, S. Harder, CCDC 2449050: Experimental Crystal Structure Determination, 2025, DOI: [10.5517/ccdc.csd.cc2n6fmy](https://doi.org/10.5517/ccdc.csd.cc2n6fmy).

